Oceanologia 63 (2021) 438—447

Available online at www.sciencedirect.com

ScienceDirect

journal homepage: www.journals.elsevier.com/oceanologia

ORIGINAL RESEARCH ARTICLE

Ocean Fronts detection over the Bay of Bengal using changepoint algorithms — A non-parametric approach

Venkat Shesu Reddem[a,*], Ravichandran Muthalagu[b], Venkateswara Rao Bekkam[c], Pattabhi Rama Rao Eluri[a], Venkata Jampana[a], Kumar Nimit[a]

[a] *Indian National Centre for Ocean Information Services, Hyderabad, India*
[b] *National Centre for Polar and Ocean Research, Vasco-da-Gama, India*
[c] *Jawaharlal Nehru Technological University, Hyderabad, India*

Received 26 October 2020; accepted 12 May 2021
Available online 26 May 2021

KEYWORDS
Ocean fronts;
Satellite imagery;
Contextual median filter;
Changepoint detection

Abstract Oceanic fronts are regions over the oceans where a significant change in the characteristics of the water masses is observed. Advanced Very High Resolution Radiometer (AVHRR) satellite imagery over the Bay of Bengal shows regions that are populated by frontal structures. Over the Bay of Bengal, some of the strongest gradients in temperature and salinity are observed. In recent years, there has been a tremendous growth in the availability of satellite imagery and the necessity of automated fast detection of the frontal features is needed for services like potential fishing zones over open oceans. In this article, an algorithm to infer oceanic fronts over the Bay of Bengal is described using changepoint analysis. The changepoint algorithm is combined in a novel way with a contextual median filter to detect frontal features in AVHRR imagery. The changepoint analysis is a non-parametric technique that does not put thresholds on the gradients of brightness temperatures of the satellite imagery. In the open oceans, the gradients of temperature and salinity are not sharp and changepoint analysis is

* Corresponding author at: Indian National Centre for Ocean Information Services, Hyderabad, India.
E-mail address: venkat@incois.gov.in (V.S. Reddem).
Peer review under the responsibility of the Institute of Oceanology of the Polish Academy of Sciences.

Production and hosting by Elsevier

https://doi.org/10.1016/j.oceano.2021.05.003

found to be a useful complementary technique to the existing front detecting methods when combined with contextual median filters.

1. Introduction

Satellite imagery over the oceans shows the huge water expanses in a completely different perspective. In general, the sea surface is characterized by regions or pockets of water masses which show sharp changes in temperature, salinity, density or in general a parameter of specific interest like e.g. chlorophyll concentration. These features are collectively referred to as ocean fronts (Belkin and O'Reilly, 2009). Knowledge of their formation, propagation and eventual decay over time and spatial scales is useful to understand processes like mixing. It is also linked to processes like upwelling, downwelling and development of near-surface currents (Halliwell Jr and Mooers, 1979; Williams and Follows, 2011). In the near-surface layers, wind and convection are the primary forcing parameters by which there is the mixing of the water masses across the horizontal and vertical direction (Eladawy et al., 2017).

Mixing in the upper surface is complex and occurs over a wide spectrum of temporal and spatial scales of motion (Hopkins et al., 2010). The water masses on either side of a frontal structure can retain their properties over short time scales (days to weeks). A number of studies show that the duration of fronts and their decay is proportional to the slope of the gradients of the properties e.g, sea surface temperature, and salinity among others. Fronts also influence the optical and biogeochemical structure (Telesca et al., 2018) of the water masses significantly. For example, the upwelling (Krężel et al., 2005; Lehmann et al., 2012) and divergence of the cyclonic eddies make the thermocline shallow and thus enhance the nutrient entrainment to the photic depths (Gurova et al., 2013; Williams and Follows, 2011). The gradients of temperature and salinity generally vary over scales as small as 1 m to 10—100 km (McWilliams, 1985; Qiu et al., 2017). The knowledge of the frontal structures and their role in air-sea interaction processes is useful to study climate variability, augment operational weather services and forecasting, identify potential fishing zones, etc. (Lehmann et al., 2012).

There are limited studies on robust automatic identification of frontal features (Cayula and Cornillon, 1992, 1995). Further, satellite imagery are seldom clean and a significant amount of pre-processing has to be carried out to minimize noise before implementing front detection algorithms for automatic identification of frontal features. In addition to the noise, problems related to missing data, presence of clouds, sensor inaccuracies, atmospheric corrections need to be carefully addressed in any automated front detection algorithm.

Using AVHRR and SeaWiFS data Wang et al. (2010) studied the spatio-temporal relationship between the sea surface temperature and the migration of the squid fisheries. Productive squid fisheries were related to the warm SST. The maps of sea color fronts and squid fisheries migration are found to be correlated in the North Pacific Ocean region. Recently Yu et al. (2017) used a data-adaptive edge detection and threshold segmentation technique to detect oil spills in Synthetic Aperture Radar (SAR) imagery. Stramska and Aniskiewicz (2019) used satellite imagery to study the variability of the sea level driven by the weather patterns named the major Baltic events (MBE's), over the Baltic and the North Sea. During the major Baltic events, there is a large influx of salty waters into the North Sea and the Baltic Sea, which modulates the local air-sea interaction processes.

The Bay of Bengal is often regarded as one of the most unique oceanic regions in the world. Many of the major rivers of south Asia such as the Ganges, the Brahmaputra and the Irrawaddy empty huge volumes of fresh water into the Bay of Bengal. The Asian subcontinent and the Bay of Bengal also experience significant amounts of rain during the Indian summer and winter monsoon (Vinayachandran et al., 2013). Every year this is the region of major cyclone activity and the cyclones and monsoon together bring a huge amount of precipitation. The freshening and transport of varying density masses in the upper surface of the Bay then give rise to regions of sharp temperature and salinity gradients. A number of in-situ observations from research ships and moorings deployed in this region show that the temperature and salinity induced gradients are shallow and strongly stratified especially near the head Bay region.

Many of the contemporary state-of-the-art weather and climate model simulations even at very high resolutions cannot simulate the frontal structures. Point location observations such as those from moorings buoys and research ships do not show processes at these larger spatial scales. Although data from Argo floats have proved to be very useful to add to the existing observations database, their coverage is restricted only in the centre of the basin and thus miss out on scientifically and strategically important regions such as northern Bay and the regions along the Indian shoreline. In this context, remote sensing satellites have the capability to cover basin-wide observations and provide a basin-scale view of the near-surface air-sea interaction processes. In this direction, Advanced Very High Resolution Radiometer (AVHRR) data of sea surface temperature (SST), altimetry, and ocean colour is routinely collected and disseminated by various international agencies.

In this paper, an innovative approach to detect temperature driven frontal structures from remotely sensed SST data is described. Section 2 briefly describes many of the feature extraction methods from images to complement this article. These methods are widely used by the image processing community and are described here for

completeness. Section 3 details a novel contextual median filter with particular reference to the algorithm proposed by Belkin and O'Reilly (2009). A contextual median filter partially overcomes many of the limitations of the various image processing filters described in section 2. Results on the changepoint methodology for feature detection in AVHRR satellite imagery is described in section 4. Here the necessary background and details on the advantages related to changepoints are also described. The main conclusions from this study are given in section 5.

2. Edge detection algorithms

From an oceanographic context and applications, there are relatively few studies on the extraction of features from satellite imagery. However, analysis of satellite imagery poses a number of challenges because of the heterogeneous nature of the data (image matrix); for example, gaps in the image matrix are common and seldom the images are noise-free. Further, small scale features get degraded when the images are processed by standard image processing filters (Gonzalez et al., 2004; Petrou and Petrou, 2010). Sub-pixel cloud contamination is another major source of error while computing the gradients of fields like temperature, salinity, chlorophyll, etc. The gradient operators also preferentially amplify the noise from the sub-pixel clouds. After the images are processed to an acceptable level of quality which is often subjective, further analyses related to morphological changes and patterns are carried out by different feature detection algorithms. Some of the commonly used morphological image processing algorithms and edge detectors are briefly described in this section. They can be loosely categorized but not limited to (a) derivative based edge detection methods (Holyer and Peckinpaugh, 1989; Simpson, 1990); (b) gradient-based thresholding techniques (Oram et al., 2008); (c) detection based on statistical measures and histogram analysis (Cayula and Cornillon, 1992); (d) surface fit procedures (Hopkins et al., 2010).

Derivative based edge detectors rely on locating the gradient discontinuities in the images. Roberts Cross, Prewitt, Sobel and Canny are some widely used first order edge detectors. In this derivative based edge detection method, the differencing horizontal edge points in the image matrix show the vertical changes in the intensity of the pixels and the horizontal edges. Very briefly, the horizontal edge detector is computed as $E_{X_{x,y}} = |P_{x,y} - P_{x+1,y}| \; \forall \; x \in 1, N-1; \; y \in 1, N$, where $P_{x,y}$ is pixel intensity at x, y location ($P_{x+1,y}$ is pixel upon forward marching 1 pixel in x direction). A vertical edge detector differences vertically adjacent points and thus detects horizontal edges. The horizontal intensity changes are given as $E_{Y_{x,y}} = |P_{x,y} - P_{x,y+1}| \; \forall \; x \in 1, N; \; y \in 1, N-1$. The horizontal and vertical edges together are detected as $E_{XY_{x,y}} = |2P_{x,y} - P_{x,y+1} - P_{x+1,y}| \; \forall \; x, y \in 1, N-1$. This differencing operator is called as a filter or a mask and is convolved with the image matrix to detect the edge points.

Most of the edge detectors are derived from the above representation and some of these are briefly outlined here. The Kirsch operator is a non-linear edge detecting operator. A single kernel mask (Kirsch, 1971) is used to find the maximum pixel strength along the compass directions, i.e., along the North, North-West, West, South-West, South, South-East, East and North-East. The maximum magnitude of the pixel intensity along all the directions are considered as the edges. The Robinson edge detection method (Robinson, 1977) is similar to Kirsch algorithm but is easier to implement. The filters (masks) in Robinson edge detection method are symmetrical about their directional axis. The directional axis is taken as the axis with the zeros. The matrix coefficients of the mask are symmetrical $\{-2, -1, 0, 1, 2\}$. For example, for the north direction, the matrix coefficients row-wise are [−1,0 1; −2 0 2; −1 0 1]; similarly, for the north-west direction, the matrix is [0 1 2; −1 0 1; −2 −1 0] and likewise the coefficients for the other directions can be constructed (Robinson, 1977). Because of the symmetry of the filter, only four masks need to be computed for this edge detection filter.

The Sobel edge detector computes the 2-D spatial gradients and gives more weights to regions where the gradients are strong. These strong spatial gradients correspond to the edges. Sobel operator computes the absolute gradient at each point of the grey scale image. In many applications, the location and not the intensity of the feature boundary is found. Similarly, the Susan edge detector algorithm relies on a predetermined window that is centered on each pixel and applies a locally acting set of rules to get an edge response.

The Roberts cross algorithm (Roberts, 1965) differentiates the pixels across the diagonals to estimate the horizontal and vertical edges. The filters are $M^+ =$ [0 1; −1 0] and $M^- =$ [1 0; 0 −1]. The edge pixels $E_{x,y}$ is the maximum of the two values derived by convolving the masks M^+ and M^- at the image point $P_{x,y}$ where $P_{x,y}$; is the pixels of the image matrix. The edge points $E_{x,y}$ are obtained by convolving the masks with the image i,e., $E_{x,y} = \max \{|M^+ * P_{x,y}|, |M^- * P_{x,y}|\} \; \forall \; x, y \in \{1, N-1\}$. Likewise, the prewitt edge algorithm uses a 3 by 3 mask and edges are estimated by locally averaging the pixel intensities. The rate of change of image intensity along the x, y directions are given by the masks $M^x =$ [0 1 −1; 1 0 −1;1 0 −1] and $M^y =$ [1 1 1; 0 0 0; −1 −1 −1]. The orientation of the edge is estimated as $\tan^{-1}(M^x/M^y)$.

The Canny edge detection algorithm is a very popular method (Canny, 1986) and it is often referred to as an optimal edge detector. An optimal detector's response to noise is small. In this algorithm, a Gaussian smoothing of the image is carried out as a preliminary step. Canny edge detection algorithm also has good localization properties. Good localization implies that the true edges in the images are preserved to large extent. True edges are identified by a technique called non-maximal suppression of the pixels. The non-maximal suppression of the pixels generates thin lines of edge points at the correct places. Suitable two-level thresholding with hysteresis is used to connect the edge pixels.

The Marr-Hildreth edge detector is a gradient based operator based on the computation of the Laplacian of an image (Nadernejad et al., 2008). It implements the idea that a step difference in the intensity of the image can be represented as a zero crossing in the second derivative of the image. In noisy images, when gradient-based detection is poor other techniques use the classification of pixels or windows of data and some form of statistical

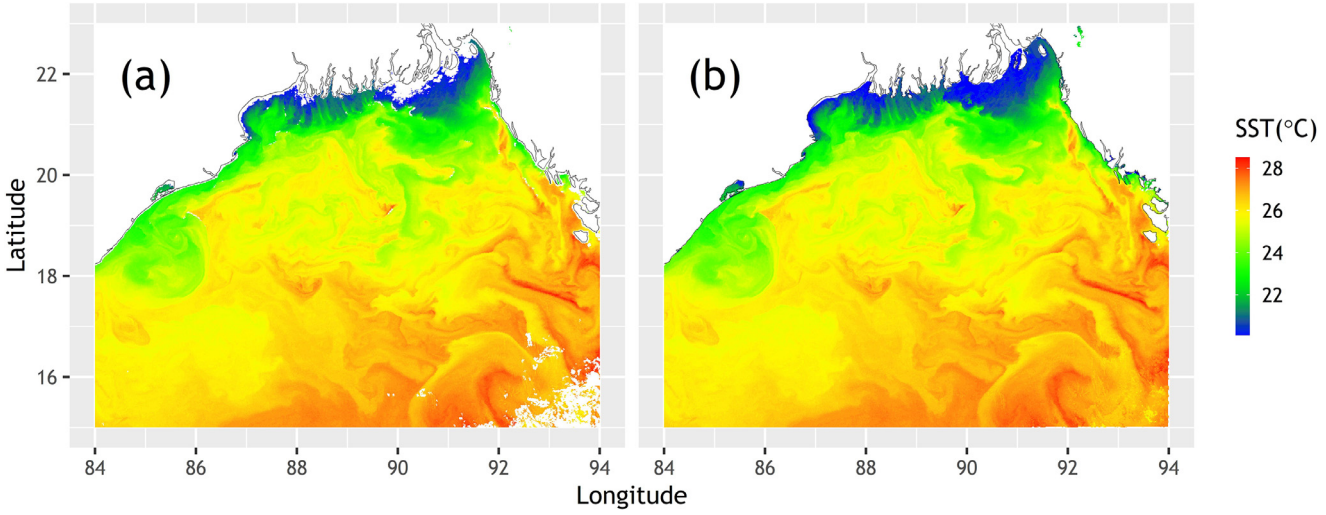

Figure 1 (a) AVHRR imagery over the head bay region of Bay of Bengal on 10th January 2018; (b) contextual median filtering of the AVHRR image.

or probabilistic analysis to determine the presence of a front. Few studies along these lines from an oceanographic fronts detection context include mathematical morphology algorithms (Krishnamurthy et al., 1994; Lorbacher et al., 2006), wavelet-based approach (Simhadri et al., 1998), and ordered structural edge detectors of Holland and Yan (1992). The major obstacle in this algorithm is to differentiate between small scale features and noise. In the next section, a contextual median filter is described which preserves the edges but at the same time does not degrade the small-scale features in the satellite imagery.

3. Data and methods

The northern Bay of Bengal region was selected as a study area. This region is remarkable for its variability. On the eastern side is the presence of the East India Coastal Current (EICC) which traverses along the east coast of India, on the north is the steady influx of fresh water from the rivers of the Indian subcontinent, on the west side is the sustained upwelling from Rossby and Kelvin waves and in the centre is the Subtropical Anticyclonic Gyre (Schott and McCreary Jr., 2001). In addition, there is the Southwest and the Northeast monsoon which bring a tremendous amount of rain and momentum flux into the ocean. This complex feedback among various processes transforms into highly complex near-surface upper ocean layers and eddy structures and fronts. The data for this study is the Sea Surface Temperature (SST) at one kilometer resolution from Advanced Very High Resolution Radiometer (AVHRR) Imagery. Figure 1(a) shows an AVHRR SST image of January 10, 2018 over Northern Bay of Bengal.

4. Contextual median filter

Noise minimization in images is effectively handled by median filters. When a median filter is implemented across a 1D array of the image matrix, the filter replaces the central value of the sliding window by the median of the 1D array. However, the application of the median filter gives rise to a problem called extremum alteration, in which the pixels of high intensity get reduced (Cayula and Cornillon, 1992, 1995). The features i.e., the pixels of higher intensity therefore become averaged to smaller values, degrading the sharp edges. This degradation of the features because of the use of the median filter defeats the very purpose of feature extraction. For example in feature extraction from chlorophyll data, the sharp peaks in SST which corresponds to local chlorophyll blooms, while ridges correspond to chlorophyll enhancement at fronts. The peaks and ridges need to be preserved in the images for proper identification of features. The filter is therefore required to be both context sensitive and selective. Also, the images have to be pre-processed to fill sparse data regions and reduce background noise in the imagery.

For oceanographic applications with a focus on the study of fronts from satellite imagery, a contextual median filter was previously proposed by Belkin and O'Reilly (2009). Very briefly a contextual median algorithm acts as a feature-preserving, scale-sensitive filter and is useful to detect sea surface temperature fronts from AVHRR satellite imagery. In this article, the contextual median filter is used for preprocessing the images and it is similar to the Canny edge detection algorithm, where a gaussian smoothing is carried out before applying a Sobel filter to detect edges. The contextual median filter is also found to improve the signal to noise ratio of the AVHRR images.

In this article the contextual median filter is implemented on the image matrix by first taking a 5 $\times$ 5 pixels sub-matrix and by finding the peak intensity across the possible dimensions of the sub-matrix. That is, across each north-south, east-west, north-west to south-east and north-east to south-east directions with respect to the centre pixel of the sub-matrix. For each of the directions, when the difference of the pixel value is 5 points (on a 0—255 scale), the sub-matrix is labelled as peak5. That is, the label peak5 implies the presence of a sharp boundary (peak in intensity) over a 5 $\times$ 5 pixel window sub-matrix. In the next step, the peak extraction method is carried for a smaller window of 3 $\times$ 3 pixels. For the 3 $\times$ 3 pixel window this

is done over two dimensions. When the center pixel of the 3×3 sub-matrix has a 3 point difference compared to the rest of the 5×5 sub-matrix surrounding it, the pixel is labelled as peak3. The label peak3 is defined as the peak over a 3×3 window (sub-matrix). These two labels, i.e., peak3 (mean peak intensity in a 3 by 3 pixel matrix) and peak5 (mean peak intensity in a 5×5 pixel matrix) are used to define an indicator function. If the peak5 exists, the value of the pixel is not changed, if the peak5 does not exist, the value is labelled as peak3. This contextual median filter is applied on the centre pixel of the sub-matrix so that the filter preserves the edges and minimizes the noise. This filter is repeatedly applied to the input image until there are no changes in data values or number of iteration does not exceed $(N-2)/2$, where N is the number of data points in the 1D array to be filtered.

Cloud free observations are difficult during the monsoon season. During the winter the atmosphere is relatively cloud free. However, the AVHRR imagery does have data gaps even during the winter season which need to be filled before detecting the changepoints in the image matrix. For this the median of the previous two images are used to fill in the gaps in the data. Figure 1(b) shows an example of gap filled image matrix.

In the next section, the changepoint algorithm to detect ocean frontal features is detailed.

5. Edge detection using changepoints

Changepoints are defined as instances in time, such that the statistical properties of the time series show significant differences before and after a given instance. One of the earliest references on changepoint detection goes back to Page (1954) with applications in the domain of manufacturing industry and production quality control. Changepoint analysis and detection has been called by different names in different fields of study. They are also often referred to as segmentation in imagery, structural break points in time series (Chen and Gupta, 2011). In the paragraph to follow, the changepoint algorithm is described.

Let the time series be represented as $\{x_1, x_2, ...x_n\}$. This data are taken to be an instance of a distribution with parameter vector θ. Assume that there occurs a change in properties of the time series at some time τ. A change is defined in terms of the difference in properties between these two segments. A change in the structure of the time series can arise from a change in the mean, or a change in variance or some other parameter change in the distribution of the underlying data (Chen and Gupta, 2011; Killick and Eckley, 2014).

It assumed that the time series can be represented as $x_j = f(t_j) + e_j; 1 \leq j \leq n$; here the $f(t)$ is a function which is representative of the distribution from which x_j is derived and e_j is the time sequence of errors. It is assumed that the function f is piecewise constant, and there exists changepoints such that $f(t) = \mu_k \; \forall \; p_{k-1} < t < p_k$. When the error terms are a sequence of independent and identically distributed gaussian variables, then x_j is also a sequence of independent gaussian variables. The time series is then modeled as $x_j \sim \mathcal{N}(\mu_k, \sigma^2)$ for $p_{k-1} < j < p_k$. The model depends on the parameters $(\theta = \mu_1, \mu_2, ...\mu_m; \sigma^2, p_1, p_2, ...p_m)$. A likelihood function is then constructed as $\mathcal{L}(\theta; x_1, x_2, ...x_n) = \mathcal{P}(x_1, x_2, ...x_n, \theta)$, where $\mathcal{P}$ is the probability density function.

The likelihood ratio $\mathcal{L}_k/\mathcal{L}_{k-1}$ of successive time series segments across $k-1; k$ checks the goodness of fit of two competing statistical models based on the rates of their likelihood. The goodness of fit of one model is found by maximization over the entire parameter space and the other fit is found by imposing a constraint. The constraint is the null hypothesis. If the null hypothesis is supported by the observed data, the two likelihoods would not differ by more than the sampling error. A cost function is then associated with each segment of the data. The cost of segmentation is the sum across each of the segments. The segmentations are inferred through minimization of the segmentation cost. Multiple changepoints in the time series are identified by minimizing the cost function $\mathcal{C}$, which is taken as the negative of the log of the likelihood ratio. Across multiple segments of data, the cost function is simply the sum of the individual segments.

$$\sum_{n=1}^{m+1} \left[\mathcal{C} x_{p_{i-1}+1:p_i)} \right] + \beta f(m)$$

In the above equation $\mathcal{C}$ represents the cost function for a segment and $\beta f(m)$ is a penalty to guard against over fitting. Different cost functions are used in changepoint detection such as negative log-likelihood (Horváth, 1993) quadratic loss and cumulative sums, or those based on both log-likelihood and length of segment (Zhang et al., 2010).

The solution space of the changepoints is to be made optimal for efficient search. Jackson et al. (2005) proposed an optimal search algorithm. An efficient implementation of the optimal partition algorithm (Jackson et al., 2005) is provided by Killick and Eckley (2014). It is implemented by pruning the changepoint search space and thereby making the algorithm more computationally efficient. The changepoint package (Killick and Eckley, 2014) in R implements to minimize the negative log-likelihood cost function with options of using binary segmentation, segment neighborhoods and pruned exact linear time (PELT) for searching the changepoints. To avoid overfitting, the penalty functions provided in the R package include the Akaike's Information Criterion (AIC), Schwarz Information Criterion (SIC), Bayesian Information Criterion (BIC), and the Modified Bayesian Information Criterion (MBIC) (Maidstone et al., 2017).

5.1. The PELT pseudocode

The PELT pseudocode for the changepoint implementation is as follows. Details on the algorithm and computational statistics on algorithm complexity are given in Killick and Eckley (2014).

Input:

1. Time series of n data points $x_1, x_2, x_3, .., x_n$ where $x_i \in$ R.
2. Fit the data and compute the cost function $\mathcal{C}$. Generally, a log likelihood is taken as the cost function.
3. A constant K that satisfies equation $\mathcal{C}(x_{t+1:s}) + \mathcal{C}(x_{s+1} : T) + K \leq \mathcal{C}(x(t+1) : T)$

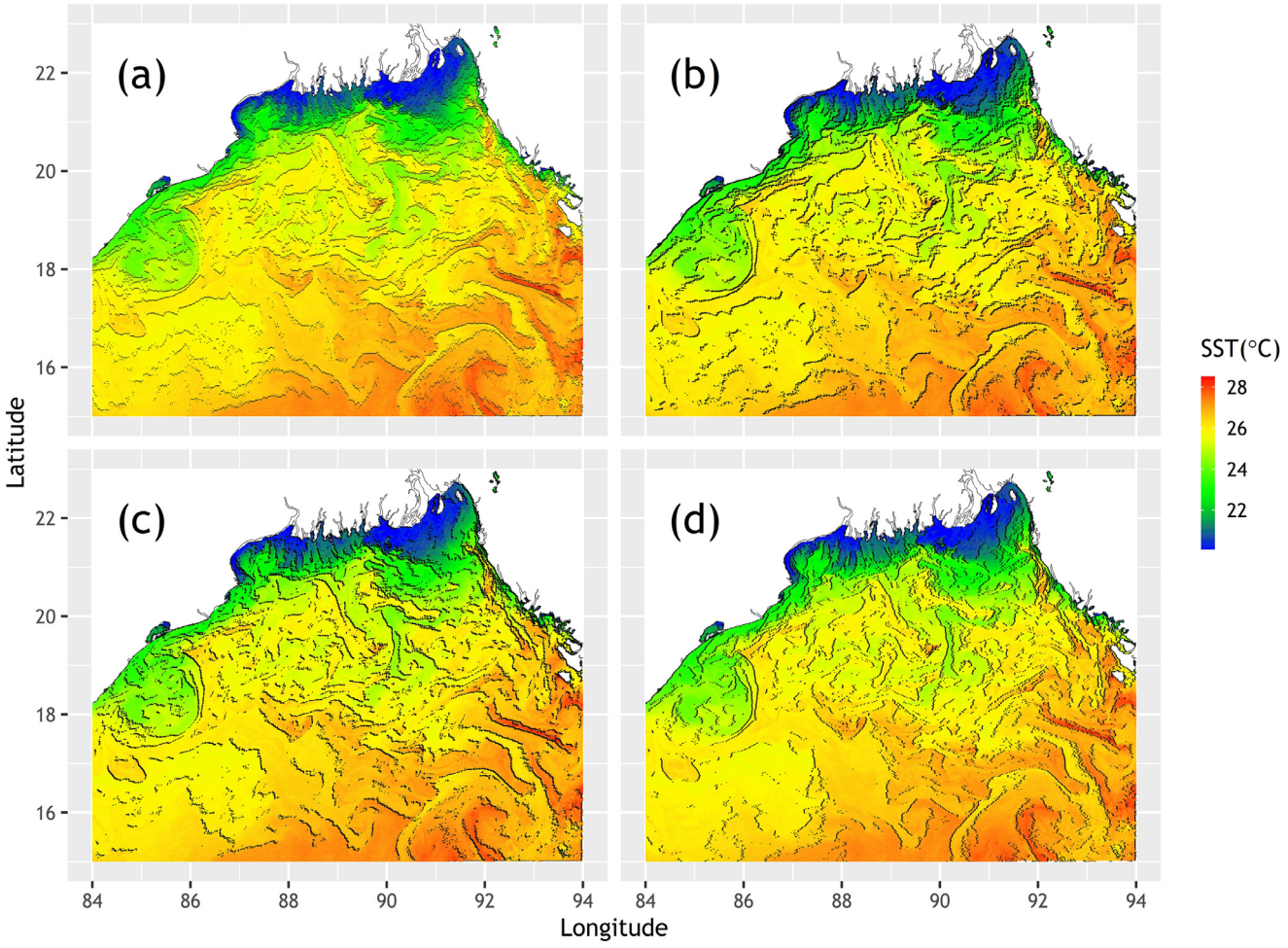

Figure 2 Changepoints in AVHRR data of Bay of Bengal on 10th January 2018 along different directions; (a) column wise; (b) diagonal wise; (c) reverse diagonal wise; (d) row wise.

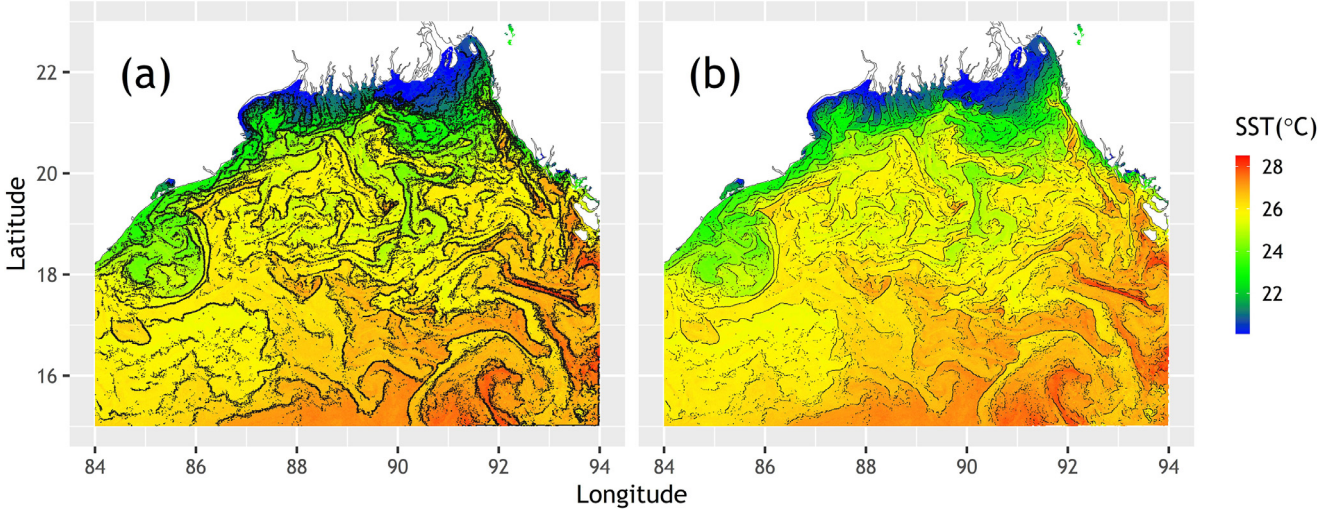

Figure 3 Total merged changepoints and thinned image in AVHRR data of Bay of Bengal on 10th January 2018; (a) merged changepoints; (b) thinned image.

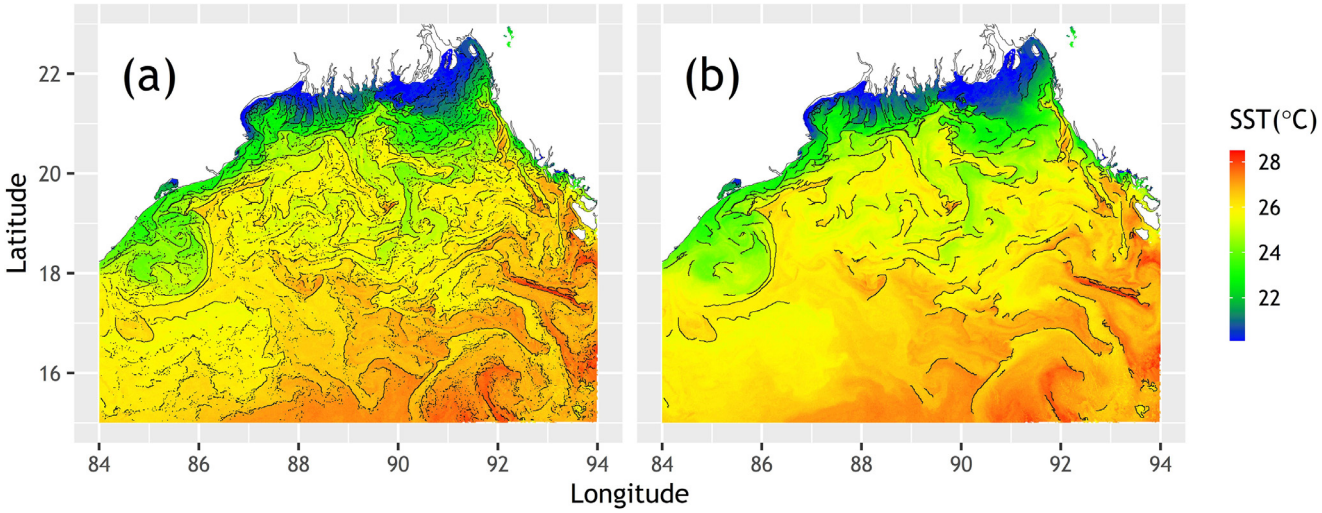

Figure 4 Merging of the frontal features and the significant fronts after suppressing the background noise and small-scale features in AVHRR data of Bay of Bengal on 10th January 2018; (a) merged fronts; (b) final fronts.

Initialize:

- Take the length of the time series as n.

Iterations: Iteration is carried out $\tau* = 1, 2, .., n$

1. Compute $F(\tau*) : \min_{\tau \in R_{\tau^*}}[F\tau + \mathcal{C}(x_{\tau+1:\tau^*}) + \beta]$
2. Compute $\tau^1 = \arg\{\min_{\tau \in R_{\tau^*}}[F\tau + \mathcal{C}(x_{\tau+1:\tau^*}) + \beta]\}$
3. Set $cp(\tau*) = [cp(\tau^1), \tau^1]$
4. Set $R_{\tau^*+1} = \{\tau^* \in R : F(\tau) + \mathcal{C}(x_{\tau+1:\tau^*}) + \kappa < F(\tau)\}$

Output:

- $cp(n)$. The list that contains the number of changepoints along the specified directions.

Edge detection using PELT involves finding changepoints in selected directions. Here we consider the north-south, east-west, northwest-southeast and northeast-southwest directions of the image matrix along which the changepoint algorithm is implemented. The changepoints obtained along these directions are directly related to the maximum likelihood of detecting edge points. The satellite imagery shows that the contrast between the land and ocean regions effects the detection of oceanic frontal structures.The land region is therefore masked such that the land edges which appear as spurious frontal regions are not labeled as ocean fronts in the final image. Figure 2 shows the composite image with changepoints which identify the frontal features along the normal and oblique directions.

Not all the changepoints showed by the algorithm are identified as potential edges or fronts. Low intensity pixels are not representative of significant fronts. The magnitude of the gradient vector of pixel intensity is used to eliminate low intensity pixels. The gradient vector is computed by implementing the Sobel operator on the image matrix which consists of two 3 × 3 convolution derivatives. The derivative masks $GX = [-1, 0, 1; -2, 0, 2; -1, 0, 1]$ and $GY = [1, 2, 1; 0, 0, 0; -1, -2, -1]$ are used to generate two vectors G_x and G_y, which contains approximations for derivatives in X and Y directions. For the original image matrix I, the derivatives are respectively, $G_x = GX \odot I$ and $G_y = GY \odot I$, where $\odot$ is a convolution operator. From these equations, the gradient magnitude (GM) and direction (GD) can be computed as $GM = \sqrt{G_x^2 + G_y^2}$ and $GD = \arctan(G_y/G_x)$. The gradient magnitude and directions in the obtained vector which are not marked as changepoints are suppressed and next the gradient magnitude of each pixel marked as changepoint is compared with the gradient magnitude of the pixel in the positive and negative gradient directions which are marked as changepoint. If the gradient magnitude of the pixel is larger compared to the other pixels, the pixel is left intact. Otherwise the changepoint pixel is suppressed and marked as not a changepoint. The convolution of the changepoint matrix with the Sobel operator gives rise to intensity directions in R^2 space. However estimating directions in R^2 space is not practically advantageous. So directions are restricted in multiples of 45°. That is, the gradients are limited to directions along $\{0^o, 45^o, 90^o, 135^o, 180^o, 225^o, 270^o, 315^o\}$ only. Figure 3 shows the merged changepoints image in panel (a). Panel (b) of Figure 3 shows the image after implementing the thinning procedure. The pixels that refer to the thinned edges correspond to the most likely regions of frontal regions.

In the next step, the edges are to be merged using some objective criteria. In the process of edge merging, the algorithm checks each edge to find whether a neighboring edge segment or pixel with a given distance of 3 pixels can be merged to form a continuum. The gradient direction is checked prior to merging the segments, to find if the gradient direction of edge pixels is less than 90°. If true, the broken edges are merged by marking the between pixels as changepoints as shown in the left panel of Figure 4.

In the final step, a thresholding selection criteria is evoked to suppress the fronts with minimal length and magnitude. To delimit the noise, fronts with length less than 10 pixels (Oram et al., 2008) are masked. Front segments with minimal length greater than 10 pixels are labeled as significant fronts. These features are shown in the right panel of

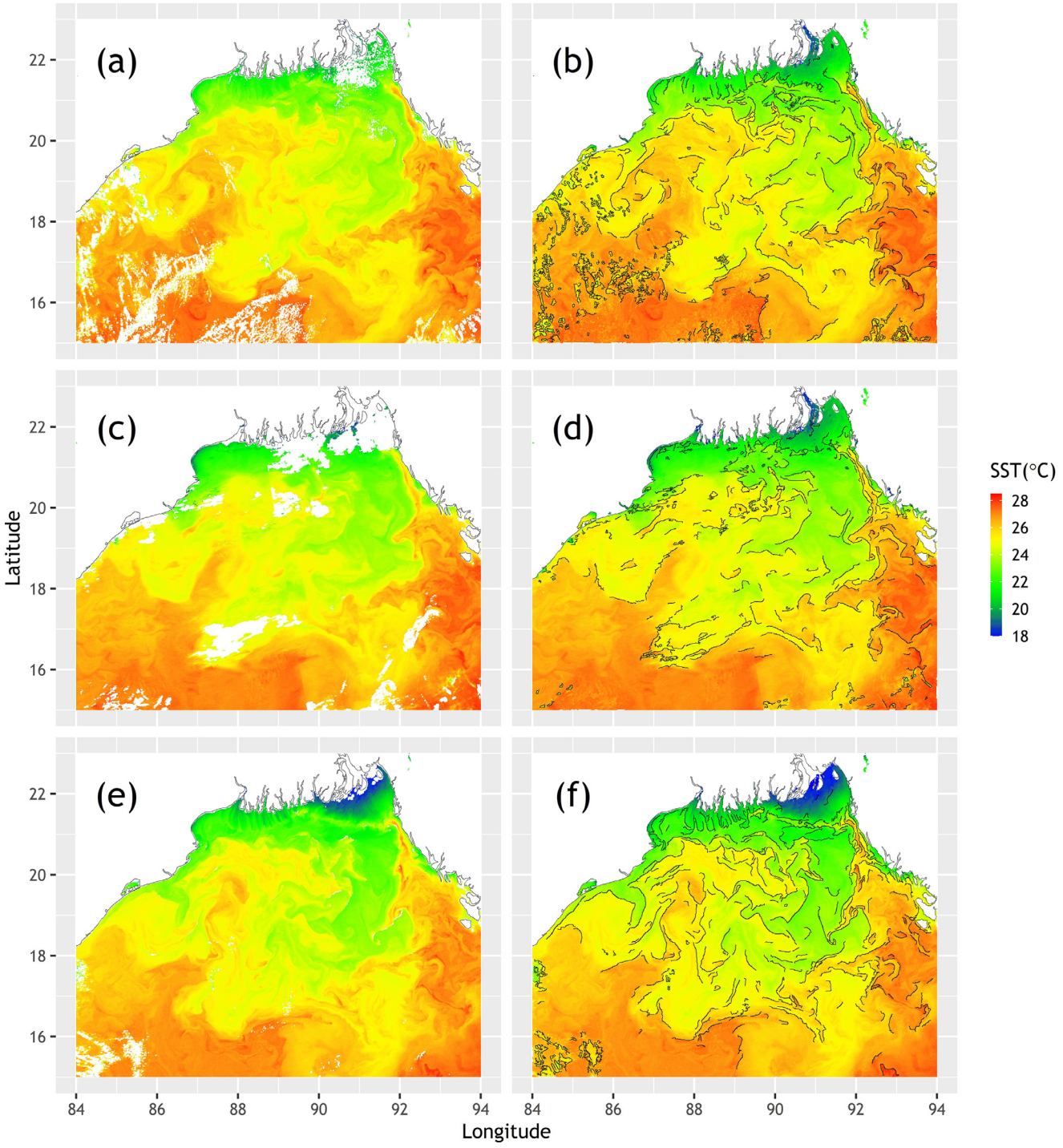

Figure 5 The satellite imagery and the fronts identified by the combination of the contextual median filter and the changepoint algorithm over 5-day period; (a) raw image of 5th January, 2013; (b) fronts of 5th January, 2013; (c) raw image of 7th January, 2013; (d) fronts of 7th January, 2013; (e) raw image of 10th January, 2013; (f) fronts of 10th January, 2013.

Figure 4. Note that the higher thresholds lead to the suppression of the smaller frontal features.

Figure 5 shows a typical example of frontal features identified by the combination of a contextual median filter and the changepoint detection algorithm over a 5-day period (5th, 7th and 10th of January 2013). The fronts are highly transient in nature. However, there exist some strong frontal structures which persist over longer periods of time, particularly those that are in the vicinity of the subtropical anticyclonic gyre (SAG).

6. Summary and conclusions

The Bay of Bengal is populated by a large density of frontal features due to its unique location and the influence of a

number of forcing factors. In this article, oceanic fronts are identified using a novel combination of the popular contextual median and a non-parametric multiple changepoint detection algorithm. It is expected that the fronts are highly transient and their identification is often subjective. This method lends some amount of objectivity in the identification procedure of the fronts. The success of the method, however, depends on proper pre-processing of the imagery. Noise and clouds can give rise to spurious fronts and this is not the ideal method for images filled with clouds. However, an inherent advantage in using the changepoint algorithm is that there is no necessity to establish a threshold value on gradients. At the first instance, the probable changepoints are found and then the procedure follows the classic front detection methods for thinning and merging. Further, the thresholding criteria on detected edge points is based on the strength of the whole front and not on individual pixel values. There is scope for improving the algorithm with multiple observation sources. Data from multiple sources can be used for further refinement of the results. Subsurface data would be available in the future and the next step is to incorporate the additional information into the change point analysis to gain more insight on the frontal features.

Acknowledgments

The authors wish to thank Dr. T. Srinivasa Kumar, Director INCOIS for the constant encouragement and support to carry out this study at INCOIS. The link https://incois.gov.in/portal/remotesensing/TERA_display.html provides the access to the data. Thanks to Dr. T.V.S Udaya Bhaskar and colleagues at the Ocean Observations and Data Management Group, INCOIS for useful discussions. This work is supported by the Ministry of Earth Sciences (MoES), Govt. of India. This is INCOIS contribution number 410.

References

Belkin, I.M., O'Reilly, J.E., 2009. An algorithm for oceanic front detection in chlorophyll and SST satellite imagery. J. Marine Syst. 78 (3), 319—326. https://doi.org/10.1016/j.jmarsys.2008.11.018

Canny, J., 1986. A computational approach to edge detection. IEEE T. Pattern Anal. PAMI 8 (6), 679—698. https://doi.org/10.1109/TPAMI.1986.4767851

Cayula, J.-F., Cornillon, P., 1992. Edge detection algorithm for SST images. J. Atmos. Ocean. Tech. 9 (1), 67—80 https://doi.org/10.1175/1520-0426(1992)009%3C0067:EDAFSI%3E2.0.CO;2

Cayula, J.-F., Cornillon, P., 1995. Multi-image edge detection for SST images. J. Atmos. Ocean. Tech. 12 (4), 821—829. https://doi.org/10.1175/1520-0426(1995)012⟨0821:MIEDFS⟩2.0.CO;2

Chen, J., Gupta, A.K., 2011. Parametric statistical change point analysis: with applications to genetics, medicine, and finance. Springer Science & Business Media.

Eladawy, A., Nadaoka, K., Negm, A., Abdel-Fattah, S., Hanafy, M., Shaltout, M., 2017. Characterization of the northern Red Sea's oceanic features with remote sensing data and outputs from a global circulation model. Oceanologia 59 (3), 213—237. https://doi.org/10.1016/j.oceano.2017.01.002

Gonzalez, R.C., Woods, R.E., Eddins, S.L., 2004. Digital image processing using MATLAB, 2nd edn. Pearson Education India.

Gurova, E., Lehmann, A., Ivanov, A., 2013. Upwelling dynamics in the Baltic Sea studied by a combined SAR/infrared satellite data and circulation model analysis. Oceanologia 55 (3), 687—707. https://doi.org/10.5697/oc.55-3.687

Halliwell Jr, G.R., Mooers, C.N.K., 1979. The space-time structure and variability of the shelf water-slope water and Gulf Stream surface temperature fronts and associated warm-core eddies. J. Geophys. Res. Ocean 84 (C12), 7707—7725. https://doi.org/10.1029/JC084iC12p07707

Holland, J.A., Yan, X.-H., 1992. Ocean thermal feature recognition, discrimination, and tracking using infrared satellite imagery. IEEE T. Geosci. Remote Sens. 30 (5), 1046—1053. https://doi.org/10.1109/36.175339

Holyer, R.J., Peckinpaugh, S.H., 1989. Edge detection applied to satellite imagery of the oceans. IEEE T. Geosci. Remote 27 (1), 46—56. https://doi.org/10.1109/36.20274

Hopkins, J., Challenor, P., Shaw, A.G.P., 2010. A new Statistical Modeling approach to ocean front detection from SST satellite images. J. Atmos. Ocean. Tech. 27 (1), 173—191. https://doi.org/10.1175/2009JTECHO684.1

Horváth, L., 1993. The maximum likelihood method for testing changes in the parameters of normal observations. Ann. Stat. 21 (2), 671—680.

Jackson, B., Scargle, J.D., Barnes, D., Arabhi, S., Alt, A., Gioumousis, P., Gwin, E., Sangtrakulcharoen, P., Tan, L., Tsai, T.T., 2005. An algorithm for optimal partitioning of data on an interval. IEEE Signal Proc. Let. 12 (2), 105—108. https://doi.org/10.1109/LSP.2001.838216

Killick, R., Eckley, I., 2014. changepoint: An R package for changepoint analysis. J. Stat. Softw. 58 (3), 1—19. https://doi.org/10.18637/jss.v058.i03

Kirsch, R.A., 1971. Computer determination of the constituent structure of biological images. Comput. Biomed. Res. 4 (3), 315—328. https://doi.org/10.1016/0010-4809(71)90034-6

Krężel, A., Ostrowski, M., Szymelfenig, M., 2005. Sea surface temperature distribution during upwelling along the Polish Baltic coast. Oceanologia 47 (4), 415—432.

Krishnamurthy, S., Iyengar, S.S., Holyer, R.J., Lybanon, M., 1994. Histogram-based morphological edge detector. IEEE T. Geosci. Remote 32 (4), 759—767. https://doi.org/10.1109/36.298005

Lehmann, A., Myrberg, K., Höflich, K., 2012. A statistical approach to coastal upwelling in the Baltic Sea based on the analysis of satellite data for 1990—2009. Oceanologia 54 (3), 369—393. https://doi.org/10.5697/oc.54-3.369

Lorbacher, K., Dommenget, D., Niiler, P.P., Köhl, A., 2006. Ocean mixed layer depth: A subsurface proxy of ocean-atmosphere variability. J. Geophys. Res. Ocean 111 (C07010). https://doi.org/10.1029/2003JC002157

Maidstone, R., Hocking, T., Rigaill, G., Fearnhead, P., 2017. On optimal multiple changepoint algorithms for large data. Stat. Comput. 27, 519—533. https://doi.org/10.1007/s11222-016-9636-3

McWilliams, J.C., 1985. Submesoscale, coherent vortices in the ocean. Rev. Geophys. 23 (2), 165—182. https://doi.org/10.1029/RG023i002p00165

Nadernejad, E., Sharifzadeh, S., Hassanpour, H., 2008. Edge detection techniques: evaluations and comparisons. Appl. Math. Sci. 2 (31), 1507—1520.

Oram, J.J., McWilliams, J.C., Stolzenbach, K.D., 2008. Gradient-based edge detection and feature classification of sea-surface images of the Southern California Bight. Remote Sens. Environ. 112 (5), 2397—2415. https://doi.org/10.1016/j.rse.2007.11.010

Page, E.S., 1954. Continuous inspection schemes. Biometrika 41 (1/2), 100—115. https://doi.org/10.2307/2333009

Petrou, M.M.P., Petrou, C., 2010. Image processing: the fundamentals. 2nd edn., John Wiley & Sons.

Qiu, B., Nakano, T., Chen, S., Klein, P., 2017. Submesoscale transition from geostrophic flows to internal waves in the northwest-

ern Pacific upper ocean. Nat. Commun. 8 (1), 1—10. https://doi.org/10.1038/ncomms14055

Roberts, L., 1965. Machine perception of 3-D solids, optical and electro-optical information processing. MIT press, Cambridge (MA).

Robinson, G.S., 1977. Edge detection by compass gradient masks. Compute. Vision Graph. 6 (5), 492—501. https://doi.org/10.1016/S0146-664X(77)80024-5

Schott, F.A., McCreary Jr., J.P., 2001. The monsoon circulation of the Indian Ocean. Prog. Oceanogr. 51 (1), 1—123. https://doi.org/10.1016/S0079-6611(01)00083-0

Simhadri, K.K., Iyengar, S.S., Holyer, R.J., Lybanon, M., Zachary, J.M., 1998. Wavelet-based feature extraction from oceanographic images. IEEE T. Geosci. Remote 36 (3), 767—778. https://doi.org/10.1109/36.673670

Simpson, J.J., 1990. On the accurate detection and enhancement of oceanic features observed in satellite data. Remote Sens. Environ. 33 (1), 17—33. https://doi.org/10.1016/0034-4257(90)90052-N

Stramska, M., Aniskiewicz, P., 2019. Satellite remote sensing signatures of the Major Baltic Inflows. Remote Sens. Basel. 11 (8), 954. https://doi.org/10.3390/rs11080954

Telesca, L., Pierini, J.O., Lovallo, M., Santamarıá-del-Angel, E., 2018. Spatio-temporal variability in the Brazil-Malvinas Confluence Zone (BMCZ), based on spectroradiometric MODIS-AQUA chlorophyll-a observations. Oceanologia 60 (1), 76—85. https://doi.org/10.1016/j.oceano.2017.08.002

Vinayachandran, P.N., Shankar, D., Vernekar, S., Sandeep, K.K., Amol, P., Neema, C.P., Chatterjee, A., 2013. A summer monsoon pump to keep the Bay of Bengal salty. Geophys. Res. Lett. 40 (9), 1777—1782. https://doi.org/10.1002/grl.50274

Wang, W., Zhou, C., Shao, Q., Mulla, D.J., 2010. Remote sensing of sea surface temperature and chlorophyll-a: implications for squid fisheries in the north-west Pacific Ocean. Int. J. Remote Sens. 31 (1718), 4515—4530. https://doi.org/10.1080/01431161.2010.485139

Williams, R.G., Follows, M.J., 2011. Ocean dynamics and the carbon cycle: Principles and mechanisms. Cambridge University Press.

Yu, F., Sun, W., Li, J., Zhao, Y., Zhang, Y., Chen, G., 2017. An improved Otsu method for oil spill detection from SAR images. Oceanologia 59 (3), 311—317. https://doi.org/10.1016/j.oceano.2017.03.005

Zhang, L., Dong, W., Zhang, D., Shi, G., 2010. Two-stage image denoising by principal component analysis with local pixel grouping. Pattern Recogn. 43 (4), 1531—1549. https://doi.org/10.1016/j.patcog.2009.09.023